

# Microstructures of GaN and $\text{In}_x\text{Ga}_{1-x}\text{N}$ Films Grown by MOCVD on freestanding GaN Templates

J. Jasinski, Z. Liliental-Weber, D. Huang<sup>1</sup>, M. A. Reshchikov<sup>1</sup>, F. Yun<sup>1</sup>, H. Morkoç<sup>1</sup>, C. Sone<sup>2</sup>, S. S. Park<sup>2</sup> and K. Y. Lee<sup>2</sup>

Materials Science Division, Lawrence Berkeley National Laboratory, Berkeley, CA 94720, USA

<sup>1</sup>Virginia Commonwealth University, Richmond, VA, USA

<sup>2</sup>Samsung Advanced Institute of Technology, P.O.Box 111, Suwon, KOREA

## ABSTRACT

We summarize structural properties of thick HVPE GaN templates from the point of view of their application as substrates for growth of nitride layers. This is followed by the results of optical and structural studies, mostly transmission electron microscopy, of nitride layers grown by MOCVD on top of the HVPE substrates. The results indicate high structural quality of these layers with a low density of threading dislocations (in the range of  $10^6 \text{ cm}^{-2}$ ). Convergent beam electron diffraction studies showed that the MOCVD GaN films have Ga-polarity, the same polarity as the HVPE GaN substrates. Structural studies of an InGaN layer grown on top of the MOCVD GaN film showed the presence of two layers, which differed in lattice parameter and composition. The upper layer, on the top of the structure had a c-lattice parameter about 2 % larger than that of GaN and contained  $10.3 \pm 0.8$  % of In. Values measured for the thinner, intermediate layer adjacent to the GaN layer were about 2.5 times lower.

## INTRODUCTION

Large area substrates for homoepitaxial growth of GaN layers have recently become available as a result of recent progress in production of thick freestanding GaN layers grown by hydride vapor phase epitaxy (HVPE) [1,2] followed by laser-assisted liftoff [3-6]. Such substrates have been successfully applied to grow GaN layers using both, metal organic chemical vapor deposition (MOCVD) [4,7] and molecular beam epitaxy (MBE) [8] methods, resulting in high quality films, as demonstrated by the high quality of their optical spectra and good electrical characteristics. In this paper we report results of structural studies obtained by transmission electron microscopy (TEM), x-ray diffraction (XRD), and photoluminescence (PL) of such GaN and  $\text{In}_x\text{Ga}_{1-x}\text{N}$  films grown by MOCVD on freestanding HVPE GaN substrates.

Fabrication of high quality  $\text{In}_x\text{Ga}_{1-x}\text{N}/\text{GaN}$  heterostructures is important because such heterostructures are used as active layers in nitride based light emitting devices. Although bright light emitting devices, and lasers from the visible to the ultraviolet region have been fabricated, the growth of high quality  $\text{In}_x\text{Ga}_{1-x}\text{N}$  films and their microstructures are still not well understood. Application of high quality freestanding GaN substrates for fabrication of  $\text{In}_x\text{Ga}_{1-x}\text{N}/\text{GaN}$  heterostructure eliminates the negative effects resulting from severe lattice mismatch associated with heteroepitaxy on sapphire, SiC and other foreign substrates.

The paper is divided into two parts. First, the microstructure and structural characteristics of HVPE GaN will be discussed. The properties of both, thin HVPE GaN layers, attached to a sapphire substrate, and thick free-standing GaN layers removed from the sapphire and prepared for use as substrates for subsequent growth of nitrides will be summarized. In the second part of the paper results of studies, performed on GaN and  $\text{In}_x\text{Ga}_{1-x}\text{N}$  MOCVD layers grown on the freestanding HVPE GaN templates will be presented.

## FREESTANDING HVPE GaN

Freestanding GaN substrates used in this investigation were produced by laser lift-off of thick HVPE GaN layers from the sapphire substrates on which they were grown. HVPE GaN layers have been grown on several substrates however, sapphire is most commonly used. Because of the large mismatch in the lattice parameters and thermal expansion coefficients between GaN and sapphire, a high density of misfit dislocations, with an average separation of about 20 Å is formed at the layer/substrate interface [9]. Lattice mismatch also leads to the formation of a high density of threading dislocations which are the dominant defects in HVPE GaN grown on sapphire. Threading dislocations are formed in the early stages of growth because the GaN film starts to grow in an island mode resulting in many slightly tilted/twisted GaN subgrains. Threading dislocations are formed at the subgrain boundaries due to this misorientation and possibly also as a result of point defect condensation, as suggested recently [10]. The density of threading dislocations in the sub-micrometer thick layer adjacent to the interface with the sapphire is of the order of  $10^{10} \text{ cm}^{-2}$ . Once threading dislocations are formed they propagate into the layer during further growth. Despite this high initial density of threading dislocations, their number gradually decreases, as the layer becomes thicker. This is due to interactions between adjacent dislocations resulting in annihilation or combination. However, this dislocation reduction is most efficient when dislocations are close to each other. Two dislocations can either annihilate or form a single dislocation with different Burgers vector. Therefore, in the early stages of HVPE GaN layer growth when many dislocations are inclined, due to the island growth mode, the overall density of dislocations decreases rapidly. As the distance from the substrate increases, the number of inclined dislocations decreases, compared to the number of dislocations almost parallel to the c-axis, and the rate of dislocation density reduction slows down. Our recent detailed studies showed that the threading dislocation reduction mechanism in HVPE GaN grown on sapphire is well described, as shown in Fig.1, by a  $1/h$ -scaling factor, where  $h$  is film thickness [9]. Such behavior was originally proposed for cubic materials by Speck et al. [11] and this theoretical model has been extended by Mathis et al. [12] to the case of GaN layers. From data shown in Fig.1 one can see that the density of threading dislocations is reduced by about four orders of magnitude when thick layers, with a thickness of a few hundred micrometers are grown.

The few hundred micrometer-thick freestanding HVPE GaN templates after, removal of about a one hundred micrometer thickness from the substrate side, have a density of dislocations in the range of a few times  $10^7 \text{ cm}^{-2}$  on the substrate side, and only about  $5 \times 10^6 \text{ cm}^{-2}$  on the surface side. Despite this low density of dislocations such a layer can not be used directly as a substrate for epitaxial growth due to its surface roughness caused by the presence of large hexagonal pyramids [4]. However, this roughness can be removed using mechanical polishing and dry etching followed by wet etching in molten KOH. Such a procedure results in a smooth, flat, epi-ready surface [8].

The types of threading dislocations in HVPE GaN are similar to those observed in materials grown by other methods. Three Burgers vectors:  $1/3\langle 11-20 \rangle$ ,  $\langle 0001 \rangle$  and  $1/3\langle 11-23 \rangle$  representing edge, screw and mixed-type dislocations are present. In thin layers, the densities of all three types of dislocations are similar but as the layer becomes thicker a higher fraction of mixed dislocations remains in the film [9]. Recently, we have shown that many of the screw dislocations in HVPE GaN layers have a bamboo-like structure due to a decoration of the core with small, nanometer-size, nanopipes [13,14].

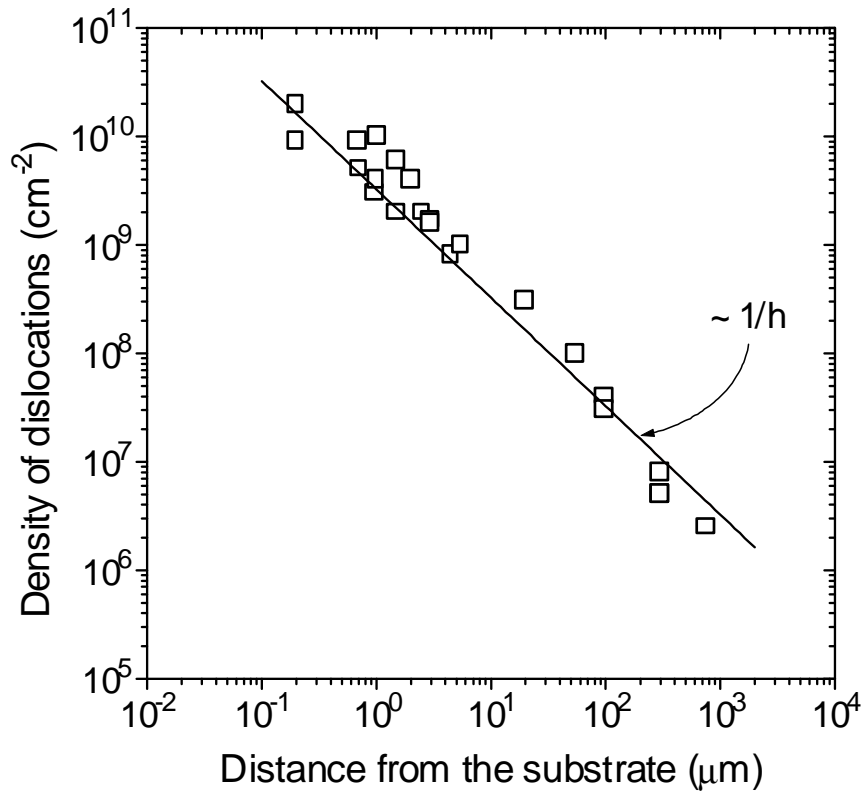


Fig. 1. Reduction of threading dislocation density in HVPE GaN (after Ref. [9]).

Extensive studies, using convergent beam electron diffraction (CBED) show that, HVPE GaN layers grow with Ga-polarity [5,9]. This means that the Ga-N bond parallel the c-axis in the growth direction is from Ga to N. In addition, no inversion domains (IDs), regions with opposite (N) polarity, were found in a large majority of the HVPE GaN layers. Only recently, we observed a freestanding GaN layer in which a high density of IDs were present only near the substrate side [9]. Their presence was shown by CBED and was supported by diffraction contrast experiments: inversion domain boundaries (IDBs), which surround IDs disappeared for g-vector perpendicular to the c-axis and were in strong contrast for g-vector parallel to the c-axis, similarly as in the previous studies of IDs in GaN [15,16]. The presence of such IDs does not have a negative impact on the quality of the free surface of the thick HVPE layer and on the quality of the subsequent layer structure grown on this surface. This is because such IDs are overgrown by the surrounding, Ga-polarity material, which apparently grows faster. In a freestanding layer, which contained such IDs, all areas of N-polarity terminated within a few tens of micrometer thickness near the substrate side. The remaining, top part of this ~200 μm-thick layer was ID-free.

Summarizing this part of the paper, all quasi-bulk, few hundred micrometer-thick, freestanding HVPE GaN templates have primarily Ga-polarity, and are ID-free near the surface side. After mechanical polishing followed by appropriate etching, such templates have very smooth, flat, epi-ready surfaces, which together with their very low density of dislocations ( $\sim 5 \times 10^6 \text{ cm}^{-2}$  on the surface side) makes them suitable candidates as substrates for epitaxial growth of nitride layers.

## MOCVD LAYERS GROWN ON FREESTANDING HVPE GaN

### Optical properties

Two MOCVD layer structures (H01 and H05) were grown for this study. Sample H01 contained a nominally undoped 2  $\mu\text{m}$ -thick GaN layer on top of a 200  $\mu\text{m}$ -thick GaN template. PL spectra from the GaN substrate and MOCVD-overgrown layer are shown in Fig. 2. Multiple sharp peaks confirm the high quality of the substrate and the layer. Donors, labeled as  $D_1$  and  $D_2$  in Fig. 2, that participate in exciton recombination, are identified as oxygen and silicon, respectively [8]. Reduction of the FWHM of the main peak from  $\sim 0.8$  to 0.47 meV after overgrowth of the thin GaN layer on the GaN freestanding substrate evidences improvement of crystal quality. Deeper analysis of the spectra will be given elsewhere.

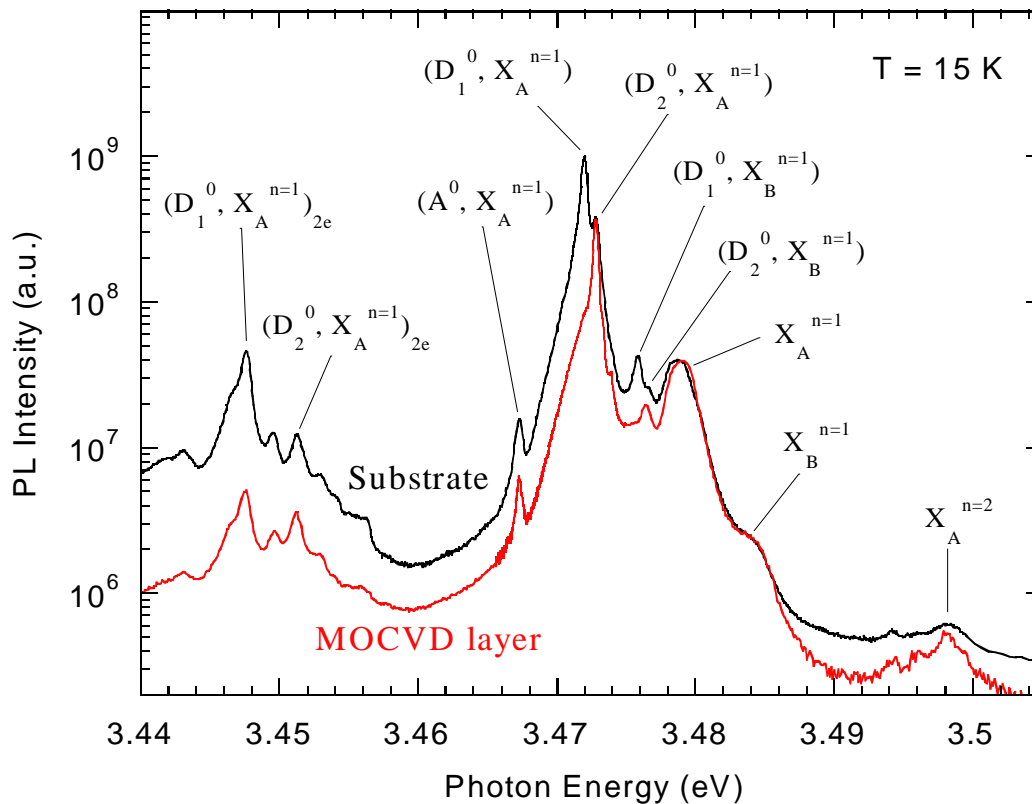


Fig. 2. Excitonic PL spectrum for HVPE-grown GaN substrate and MOCVD-overgrown GaN layer.

Sample H05 contained a nominally undoped 1.0  $\mu\text{m}$ -thick GaN layer followed by a  $\sim 30 \text{ nm}$   $\text{In}_x\text{Ga}_{1-x}\text{N}$  layer. The In mole fraction  $x$  of the  $\text{In}_x\text{Ga}_{1-x}\text{N}$  layer was estimated to be 0.12 from XRD and PL spectra. The PL peaks at 3.018 and 3.474 eV with peak widths of 36 and 6.3 meV were identified at 15 K from the  $\text{In}_x\text{Ga}_{1-x}\text{N}$  and GaN layers (Fig. 3).

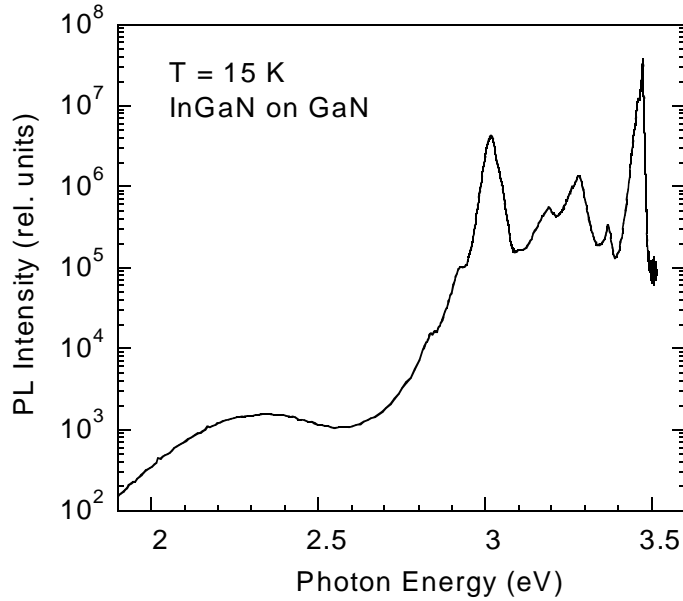


Fig. 3. PL spectrum of InGaN layer grown on top of GaN. The peak at 3.018 with two or three LO-phonon replicas is attributed to excitonic recombination in the InGaN layer. Other features are believed to be related to GaN. In addition to exciton emission (peak at 3.474 eV), shallow donor-acceptor pair band with the main peak at 3.28 eV and a broad yellow luminescence band peaking at 2.3 eV were identified.

### **Polarity**

In order to determine crystal polarity of the MOCVD layers CBED study was performed and the well-established method [17-19] was applied. This method uses the asymmetry of the intensity distribution between the (0002) and (000 $\bar{2}$ ) diffraction discs of the [1 $\bar{1}$ 00] zone axis CBED pattern. Because the intensity distribution within the specific CBED disc depends not only on the crystal polarity but also on the TEM specimen thickness. The intensity distribution within the central - (0000) - disc was first used in this method to determine the specimen thickness. Then a CBED pattern was simulated for this specific thickness to match the asymmetrical intensity distribution within the (0002) and (000 $\bar{2}$ ) diffraction discs, which allows determination of the crystal polarity.

Results obtained from application of this method for samples H01 and H05 are shown in Fig.4. Experimental CBED patterns (shown in Figs 4(b) and 4(f), respectively) were recorded in the areas marked by the electron beam on images shown in Figs 4(a) and 4(e), respectively. Simulated CBED patterns for 220 nm and 205 nm sample thickness are shown in Figs 4(c) and 4(g). A good match between experimental CBED patterns and simulated ones was obtained for these thicknesses. Both layers were shown to have grown with Ga-polarity. Schematic representation of atom arrangement along the crystal growth direction are shown in Figs 4(d) and 4(h).

Our CBED studies did not show presence of any IDs which was also confirmed by dark field imaging under two-beam conditions with g-vector parallel to the c-axis, which is sensitive to polarity change. All results indicate that both MOCVD GaN layers have uniform Ga-polarity, the same polarity as the freestanding HVPE GaN substrates used for the growth.

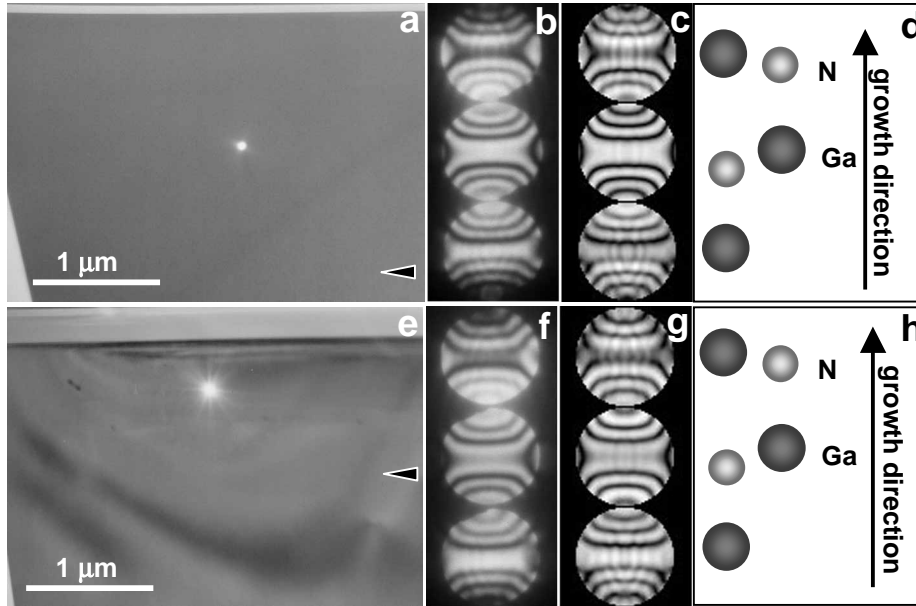


Fig.4. Polarity determination for MOCVD grown GaN layer in H01/H05 sample: (a)/(e) TEM micrograph of this layer (arrow indicates the nominal location of the interface between the layer and the freestanding HVPE GaN substrate): (b)/(f) The experimental  $[1\bar{1}00]$  zone axis CBED patterns recorded from the area marked by the beam; (c)/(g)  $[1\bar{1}00]$  CBED pattern simulated for 220 nm (205 nm) and Ga-polarity of the crystal (Note very good match between simulated and experimental patterns): (d)/(h) Schematic distribution of N and Ga atoms along the c-axis.

### Microstructure of MOCVD GaN

A TEM investigation of the MOCVD GaN layer grown in sample H01 showed very high crystal quality. First, the interface between this layer and the HVPE GaN substrate could not be detected in the TEM micrographs suggesting that there were no defects or large-scale impurities present at this interface. The only defects observed in the layer were threading dislocations with a density of the order of a few times  $10^6 \text{ cm}^{-2}$ . All these dislocations propagated from the substrate. One such dislocation is shown in Fig. 5(a) where the nominal location of the layer/substrate interface is marked by arrows.

As mentioned in the first part of this paper, screw dislocations in HVPE GaN are often decorated by small nanopipes. Here in sample H01, some screw dislocations present in the HVPE GaN substrate were decorated by such nanopipes as shown in Figs. 5(b) and 5(c). However, MOCVD growth seems to be different from that of HVPE. There are no nanopipes observed along these dislocations during the MOCVD growth (see Figs 5(b) and 5(c)).

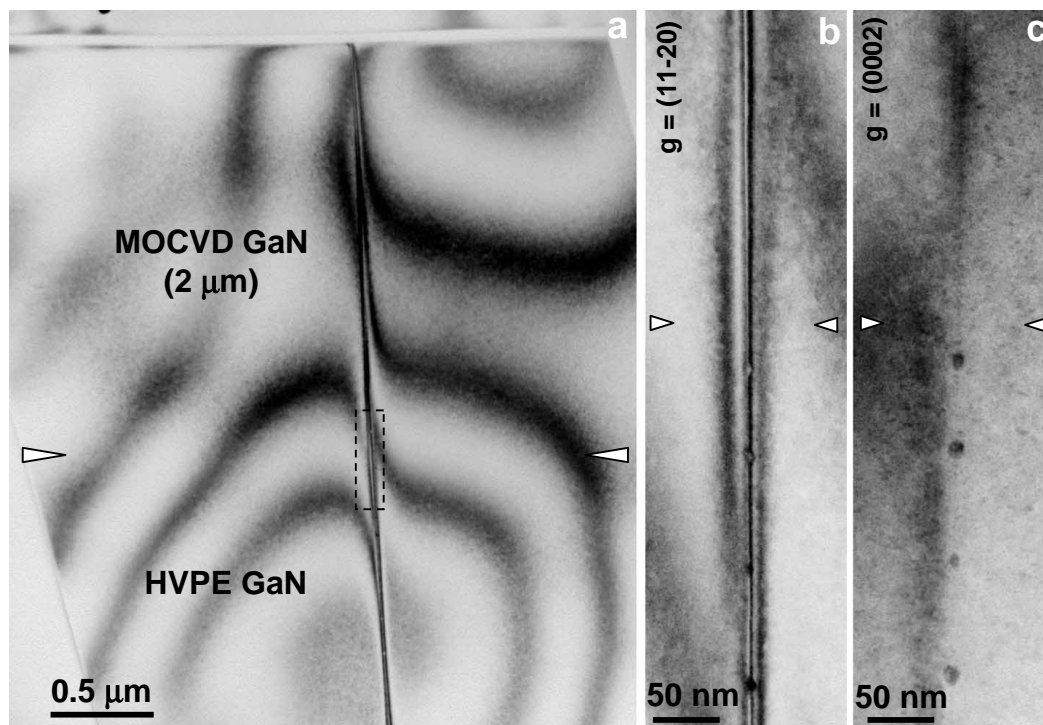


Fig. 5. (a) TEM micrograph of MOCVD layer grown in sample H01. The only defects present in this layer are threading dislocations originated from the HVPE freestanding substrate. (b), (c) Bright field TEM micrographs of the area marked in with a dotted box in Fig. 5(a) recorded for  $g$ -vector perpendicular and parallel to the  $c$ -axis. Screw threading dislocations visible in this region are decorated by small nanpipes. Notice that these nanpipes are only in the substrate HVPE GaN template (below the arrows marking the interface between the template and the MOCVD GaN layer).

Two types of defects were found in sample H05. First, there were again threading dislocations originating from the substrate, with a density of the order of a few times  $10^6 \text{ cm}^{-2}$ . Some of the threading dislocations were found to bend at the  $\text{In}_x\text{Ga}_{1-x}\text{N}/\text{GaN}$  interface, as shown in Figs 6(a) and 6(b). In addition to threading dislocations some dislocation loops (DLs), located on the  $c$ -plane were observed (see Fig. 6(a)). They were visible in strong contrast for  $g$ -vector perpendicular to the  $c$ -axis and disappeared for the  $g$ -vector parallel to the  $c$ -axis (see Fig. 6(a) and 6(c)). However, a majority of these DLs were located below the layer/substrate interface within the HVPE GaN substrate. Therefore it seems that MOCVD GaN layer in sample H05, also has a very good structural quality. As in the case of sample H01, no structural defects were observed to nucleate at the layer/substrate interface. In fact, the interface was also very difficult to detect and could only be distinguished in TEM micrographs recorded for  $g$ -vector parallel to the  $c$ -axis (see Fig. 6(d)). This suggests that some residual impurities could be present at this interface.

Summarizing, MOCVD GaN layers grown on high quality freestanding HVPE GaN substrates were found to have a high structural quality. The interface between such layers and the substrate was either undetectable or hardly detectable in TEM micrographs suggesting that there were no structural defects and only some residual impurities present and this interface. The main structural defects found in these layers were threading dislocations, originating from the substrate, with a low density in the range of few times  $10^6 \text{ cm}^{-2}$ . Small nanpipes were observed

to decorate some screw dislocations in the HVPE GaN substrates but nanopipes were not detected in the MOCVD GaN films grown on top of the HVPE layer.

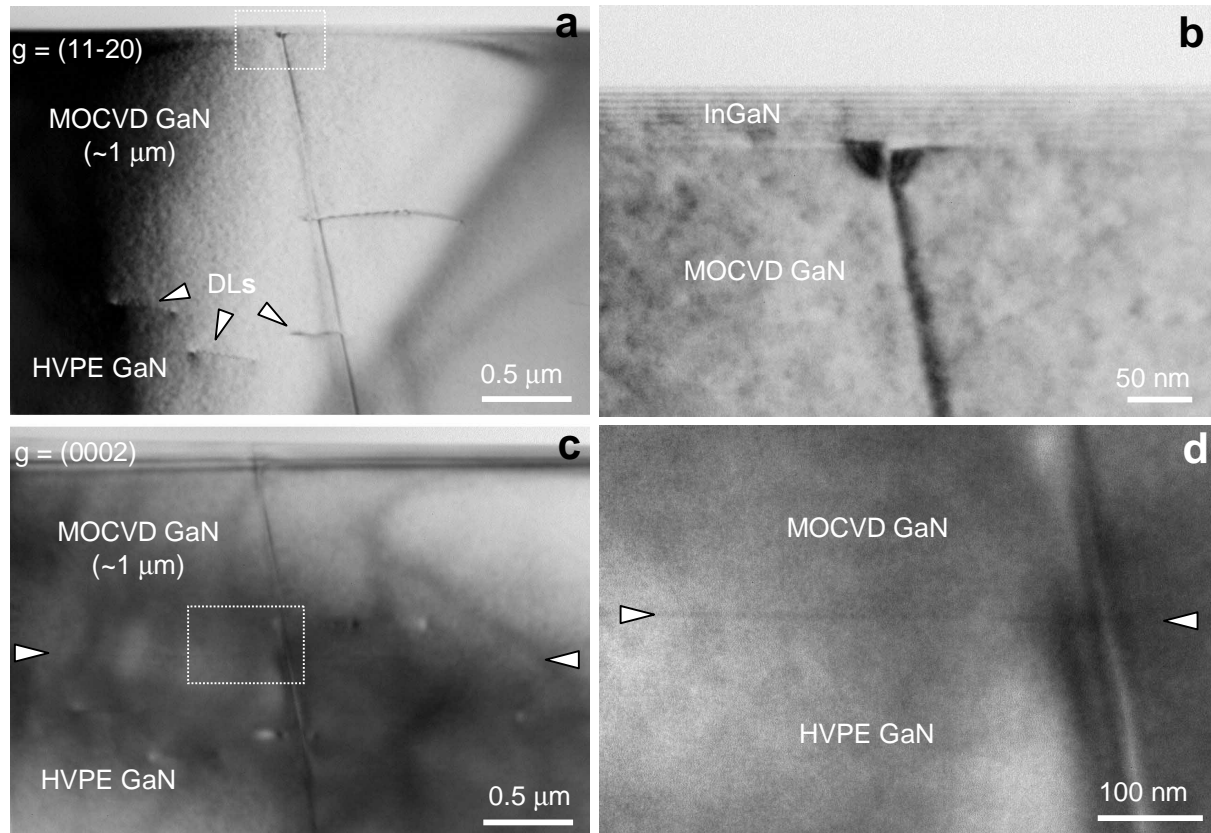


Fig.6. Microstructure of sample H05. Bright field images of the MOCVD GaN layer taken for g-vector perpendicular (a) and (c) parallel to the c-axis. (b)/(d) Larger magnification image of the area marked by a dotted-line rectangular frame in figure (a)/(c). Notice that the threading dislocation shown in figure (c) bends at the interface between MOCVD grown GaN and InGaN layers. Only a slight change of contrast [see figure (d)] is visible at the interface between the HVPE GaN substrate and MOCVD grown GaN layer suggesting that only some residual impurities could be present at this interface.

### **Microstructure of MOCVD InGaN**

The InGaN layer grown by MOCVD on top of a 1  $\mu\text{m}$ -thick MOCVD GaN layer in sample H05, was intensively studied by different microscopic techniques. Our studies indicate that this layer contains at least two sublayers with different compositions. It was first indicated by high-resolution electron microscopy (HREM) images, where a difference in contrast suggested the presence of two separate sublayers. An example of such an image is shown in Fig. 7(a), where arrows indicate the location of interfaces. The first sublayer adjacent to the MOCVD GaN layer has a thickness of about 10 nm. On top of it, there is a second layer with a thickness of about 25 nm. The location of both interfaces is also indicated on the plot, shown in Fig. 7(e), showing the brightness level in such HREM image averaged along the lines parallel to the c-planes. In this plot, in addition to fast brightness oscillations corresponding to the lattice fringing (see also inset where such oscillations are shown more clearly), there is also a change of average brightness level at a larger scale. Two well-defined thresholds are visible in positions corresponding to the

locations of both interfaces (between GaN and the first InGaN layer and between the first and the second InGaN layers). The average brightness has its highest value in the area of the GaN layer and its smallest value in the area of the second InGaN layer. Such a change of the brightness level indicates that the two InGaN layers had different In contents, the thicker layer, located closer to the surface, with lower brightness level contains more In.

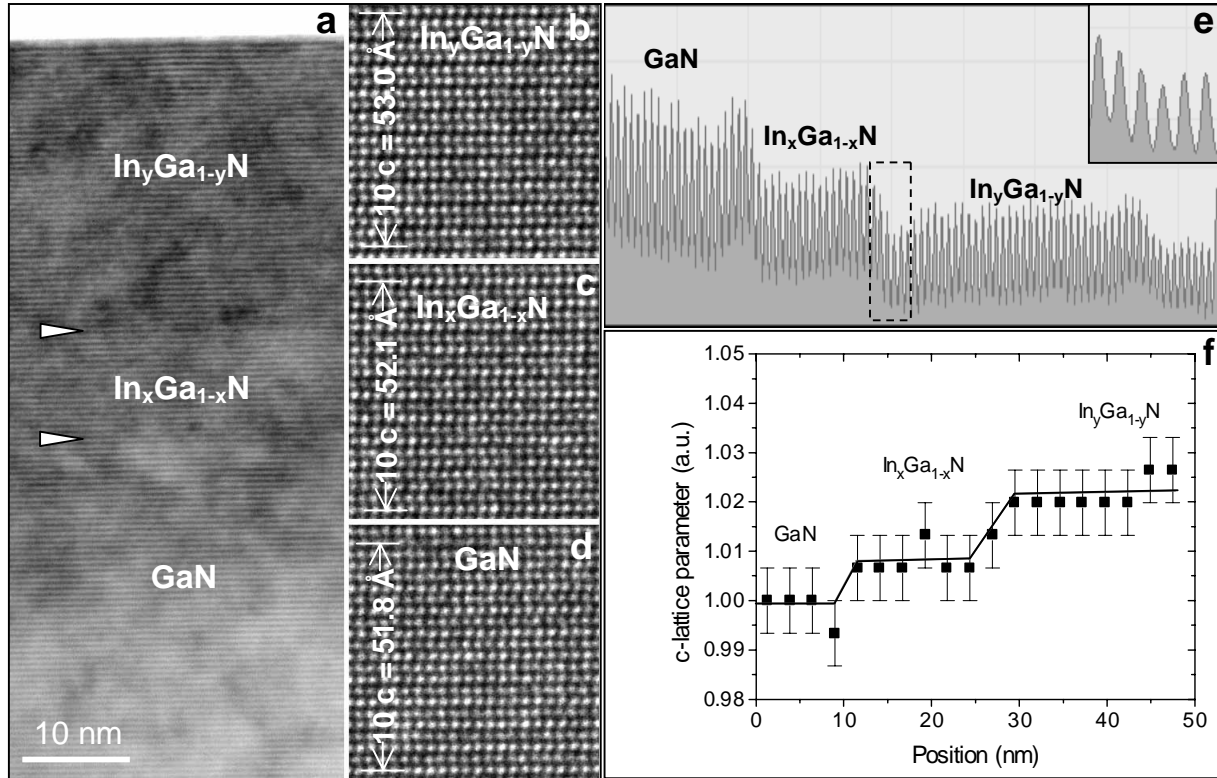


Fig. 7. (a) HREM image of InGaN/GaN layer structure – abrupt interfaces indicated by arrows suggest existence of two, well-defined InGaN layers. (b)-(d) Detailed HREM images (recorded with higher resolution than image from Fig. 7(a)) of MOCVD GaN layer and both InGaN layers. (e) Profile of the average brightness level in image shown in Fig. 7(a). Sharp oscillations represent c-lattice fringing and two thresholds indicate the location of both interfaces marked on Fig. 7(a). Inset shows c-lattice fringing oscillations from the area marked with a dotted-line rectangular frame. (f) Profile of the relative change of c-lattice parameter across the layer structure. Notice that again at least two well-defined InGaN layers (with a c-lattice parameter larger than that of GaN) are visible.

In order to measure the lattice parameter HREM images taken from all three layers (GaN and both InGaN layers) were used. Examples of such HREM images are in Figs 7(b)-7(d). The smallest c-lattice parameter was measured in the image of the GaN layer (Fig. 7(d)) and the highest in the image of the second InGaN layer (Fig. 7(b)). Results of a more quantitative analysis are shown in Fig. 7(f), where the relative change of c-lattice parameter is plotted across the layer structure. Despite a relatively high uncertainty for these experimental data, two well-defined layers with thicknesses similar to those obtained from the brightness level profile are visible. The lattice constant of the first, thinner InGaN layer in the c-direction is about  $0.7 \pm 0.5 \%$  larger than that of the GaN layer. The lattice constant of the second layer is about  $2.1 \pm 0.5 \%$  larger than that of GaN. In addition, these c-lattice parameter measurements showed also a systematically higher value (of about 3 %) in a thin layer located just below the surface (see Fig.

7(f)). This correlates well with a small additional threshold visible in the brightness level profile (see Fig. 7(e)) and suggests that the second layer can in fact be composed of two separate layers (the second one with a thickness of about 5 nm).

In order to confirm if In concentration is changing in these layers energy dispersive X-ray (EDX) line profiles were measured across the layer structure. Two sets of such profiles (measured across longer and shorter distance) are shown in Fig. 7. Ga and In profiles are shown together to see changes in the relative amounts of both elements. In addition, a profile of the background intensity change is shown as a reference. One can see from In EDX profiles that there are two distinct layers containing a significant amount of this element. The first layer has a thickness of about 10 nm and the second one, located below the surface has a thickness of about 30 nm. The second, thicker layer has about 2.5 times more In than the thinner one. Both, thicknesses and relative indium compositions agree well with our TEM results (thicknesses of ~10 nm, and ~25 nm measured from brightness level plot and about 3 times larger relative change of the c-lattice constant) confirming that there are at least two InGaN layers present in this sample.

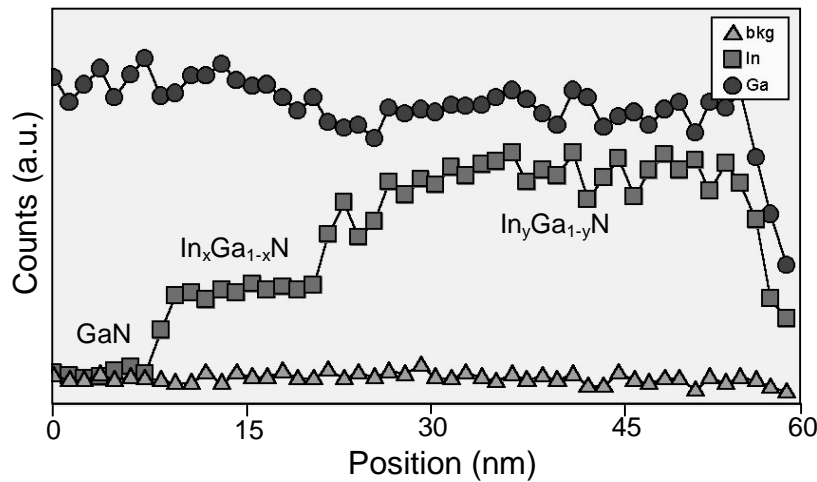


Fig. 8. EDX line profiles of Ga and In peak intensity measured across the InGaN layer grown on top of 1  $\mu\text{m}$ -thick MOCVD GaN layer. Line profile of background intensity is shown as a reference.

Because higher In concentration in InGaN layer is equivalent to lower Ga content an increase of the In peak in the EDX spectrum should be associated with a decrease of the Ga peak. This is in fact what was measured for this structure (see Fig. 8). At the left-hand side of the profiles, in the GaN layer, where there is no In detected, the Ga peak has a high, almost constant level. In the thinner In-rich layer adjacent to GaN the intensity of the Ga peak decreases slightly. This decrease is more pronounced in the thicker, top In-rich layer. The relative change of the Ga peak intensity between the GaN layer and the top layer of InGaN, was used to estimate that In content in this layer, was about  $12 \pm 2 \%$ . Taking into account the relative change of indium content between the first and the second layer a value of about  $4.8 \pm 1 \%$  for In content in the first, thinner layer was obtained. These results agree with those obtained from a quantitative analysis of the EDX spectra, where background subtraction and a model line shape fitting of the Ga and In peaks, were applied. Such a quantitative analysis provided more accurate values of In concentrations:  $4.4 \pm 0.5 \%$  and  $10.3 \pm 0.8 \%$  for the lower and the top InGaN layers, respectively.

The results obtained on InGaN/GaN heterostructure grown by MOCVD on freestanding HVPE GaN substrate indicate a very high quality of this heterostructure manifested by layer thickness uniformity and interface abruptness. Different structural studies (HREM together with quantitative analysis of c-lattice parameter and EDX measurements) indicate presence of at least two well-defined InGaN layers with thicknesses of about 10 nm and 25 nm, respectively. The thicker, top layer has an In content of  $10.3 \pm 0.8 \%$  and a c-lattice parameter about 2 % larger than that of pure GaN. Both these values are about 2.5 times larger than that measured in the thinner InGaN layer, on top of the GaN film. Uniform thickness and composition of both InGaN layers (except for a slight increase in c-lattice parameter in the upper ~5 nm-thick part of the second layer) and abrupt interfaces indicate high quality of this layer structure. Presence of these two InGaN layers suggest spontaneous vertical In localization as observed earlier [20,21]. Alternatively a sudden change in growth conditions could result in formation of two separate layers with different In contents.

## CONCLUSIONS

Defect characterization using TEM was performed for freestanding GaN grown by HVPE. It was shown that dislocation density decreases with increasing layer thickness. Such quasi-bulk, large-area (few hundred micrometer-thick) templates were used as substrates for growth of GaN and GaN/InGaN layers using MOCVD. Sharp lines in PL spectra measured for these layers indicate high structural quality, which was confirmed by structural studies. These studies show that after appropriate pre-treatment HVPE layers can have epi-ready surfaces and are suitable substrates for growth of nitride films. InGaN/GaN layer structure grown on such a substrate was found to have abrupt interfaces. A two-layer structure with two different lattice parameters and different In compositions was found in the InGaN film.

## ACKNOWLEDGMENTS

This work was supported by the Air Force Office of Scientific Research, through the U.S. Department of Energy under Order No. AFOSR-ISSA-00-0011 (Wood-Witt program). The authors would like to thank W. Swider for excellent TEM sample preparation, and Prof. J. Washburn for very fruitful discussions. TEM group (J. J. and Z. L.-W.) acknowledge the use of the facilities at the National Center for Electron Microscopy at Lawrence Berkeley National Laboratory. The work at VCU was funded by grants from AFOSR (Dr. G. L. Witt and Dan Johnstone), NSF (Drs. L. Hess and U. Varshney), and ONR (Drs. C. E. C. Wood and Y. S. Park).

## REFERENCES

1. R.J. Molnar, W. Goetz, L.T. Romano, N.M. Johnson, *J. Cryst. Growth.* **178**,147 (1997).
2. S.Nakamura, M. Senoh, S. Nagahama, N. Iwasa, T. Yamada, T. Matsushita, H. Kiyoku, Y. Sugimoto, T. Kozaki, H. Umemoto, M. Sano, and K. Chocho, *Appl. Phys. Lett.* **73**, 832 (1998).
3. M.K. Kelly, R.P. Vaudo, V. M. Phanse, L. Gorgens. O. Ambacher. M. Stutzmann, *Jpn. J. Appl. Phys.* **38**, L217 (1999).
4. C. R. Miskys, M. K. Kelly, O. Ambacher, G. Martínez-Criado, and M. Stutzmann, *Appl. Phys. Lett.* **77**, 1858 (2000).

5. J. Jasinski, W. Swider, Z. Liliental-Weber, P. Visconti, K.M. Jones, M.A. Reshchikov, F. Yun, H. Morkoç, S.S. Park, and K.Y. Lee, *Appl. Phys. Lett.* **78**, 2297 (2001).
6. J.A. Freitas, Jr. , G.C.B. Braga, W.J. Moore, J.G. Tischler, J.C. Culbertson, M. Fatemi, S.S. Park, S.K. Lee and Y. Park, *J. Cryst. Growth.* **231**, 322 (2001).
7. G. Martínez-Criado, C.R. Miskys, A. Cros, O. Ambacher, A. Cantarero, and M. Stutzmann, *J. Appl. Phys.* **90**, 5627 (2001).
8. M.A. Reshchikov, D.Huang, F. Yun, L. He, H. Morkoç, D.C. Reynolds, S.S. Park, and K.Y. Lee, *Appl. Phys. Lett.* **79**, 3779 (2001).
9. J. Jasinski and Z. Liliental-Weber, *J. Electron. Mat.*, special issue on SiC and III-V nitride materials and devices, (2002) in press.
10. V. Narayanan, K. Lorenz, Wook Kim and S. Mohajan, *Phil. Mag. A* **82**, 885 (2002).
11. J. S. Speck, M.A. Brewer, G. Beltz, A.E. Romanov, and W. Pompe, *J. Appl. Phys.* **80**, 3808 (1996).
12. S.K. Mathis, A.E. Romanov, L.F. Chen, G.E. Beltz, W. Pompe, J.S. Speck, *phys. stat. sol. (a)* **179**, 125 (2000).
13. Z. Liliental-Weber, Workshop on Extended Defects, Belize, January 27-31, 2002, unpublished.
14. Z. Liliental-Weber, J. Jasinski, J. Washburn, M.A. O'Keefe, Microscopy Society of America, Quebec City, Canada, August 4-8, 2002, submitted.
15. X. H. Wu, L. M. Brown, D. Kapolnek, S. Keller, B. Keller, S. P. DenBaars, and J. S. Speck, *J. Appl. Phys.* **80**, 3228 (1996).
16. L. T. Romano, J. E. Northrup, and M. A. O'Keefe, *Appl. Phys. Lett.* **69**, 2394 (1996).
17. Z. Liliental-Weber, C. Kisielowski, S. Ruvimov, Y. Chen, J. Washburn, I. Grzegory, M. Bockowski, J. Jun, S. Porowski, *J. Electron. Mat.* **25**, 1545 (1996).
18. J. -L. Rouviere, M. Arlery, A. Bourret, R. Niebuhr, K. -H. Bachem, *Mat. Res. Soc. Symp. Proc.* **395**, 393 (1996).
19. Z. Liliental-Weber, M. Benamara, O. Richter, W. Swider, J. Washburn, I. Grzegory, S. Porowski, J. W. Yang, S. Nakamura, *Mat. Res. Soc. Symp. Proc.* **512**, 363 (1998).
20. L. Gorgens, O. Ambacher, M. Stutzmann, and C. Miskys, F. Scholz, and J. Off, *Appl. Phys. Lett.* **76**, 577 (2000).
21. Z. Liliental-Weber, M. Benamara and J. Washburn, J.Z. Domagala and J. Bak-Misiuk, E.L. Piner, J.C. Roberts and S. M. Bedair, *J. Electr. Mater.* **30**, 439 (2001).